Utrecht University

Utrecht University
Department of Physics & Astronomy

Bachelor Thesis

Characterization of Individual Fluorophores for Application in Super-Resolution Localization Microscopy (PALM)

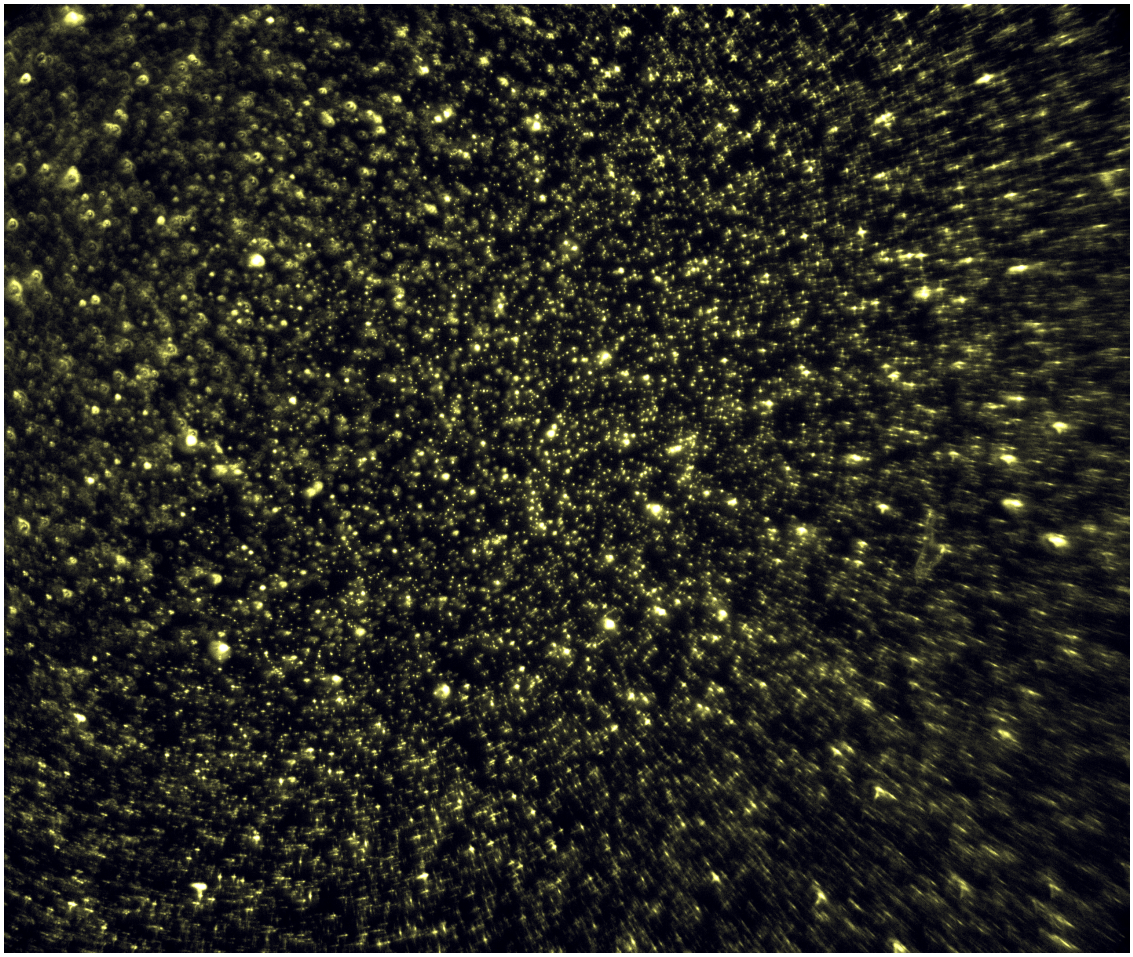

Tom Konings
supervised by
dr. Gerhard Blab
Sajjad Mohammadian PhD

June 14, 2017

"With four parameters I can fit an elephant, and with five I can make him wiggle his trunk."

- John von Neumann -

Abstract

In this thesis we characterize and analyze the single molecule fluorophore Rhodamine B isothiocyanate and core-shell fluorescent beads under dry conditions using PALM techniques. Using four different effective excitation intensities ranging from $33.1\,\mathrm{W\,cm^{-1}}$ to $1.33\,\mathrm{W\,cm^{-1}}$ we detect two distinct bleaching times (one short, one long), intensities and intensity populations for the core-shell particles. Effectively confirming the occurrence of metal-enhanced fluorescence within the beads. The process of characterizing the Rhodamine B isothiocyanate particles proved in the end to be rather unreliable due to difficulties encountered with sample contamination and the filtering of data, but shows definite room for improvement in future attempts.

Coloured in fluorescence microscopy image (approx. $277.2\,\mu\mathrm{m} \times 233.9\,\mu\mathrm{m}$) of 100 nm JP117(2) (Jantina Particle) core-shell fluorescent beads. Aberration on the sides of the image is likely caused due to a defect in the lens.

The quote John von Neumann by is cited from [1].

Contents

1 Introduction

The concept of fluorescence is one explained or at least mentioned in most elementary physics textbooks. The phenomenon of the absorption of light of a certain wavelength and accompanying emission of light with a longer wavelength is one that can be observed in many organisms and materials, both naturally occurring and synthesized. Fluorescence takes place when an orbital electron from a molecule (or atom) falls back from an excited singlet state to its ground state through the emission of a photon. As excitation of the electrons occurs through absorption of light (of which the effective spectrum of wavelengths varies greatly for different molecular structures) a continuous cyclic process of absorption and emission can be established by exposing a fluorescent particle (called a fluorophore) to a constant source of light, effectively enabling one to observe a constant emission of light (also within a spectrum of certain wavelengths) from a fluorescent particle. Not every instance of photon absorption directly results in the excitation of an electron and thus the emission of a longer wavelength photon. As such a parameter known as the quantum yield of a fluorophore can directly be defined as:

$$\Phi = \frac{\#\text{ photons emitted}}{\#\text{ photons absorbed}} \tag{1}$$

We can interpret this as being the efficiency of the fluorescence process. The quantum yield by default varies greatly for different fluorophores, but is also very strongly dependent on environmental conditions such as the temperature or the solution the particles are surrounded with.

Of course the use of the term "constant" regarding the absorption and emission depends, as is often the case in physics, on the context. Excitation and emission are not instantaneous processes and as such there is a certain time span associated with each of these aspects of fluorescence. Excitation through an incoming photon typically occurs in femtoseconds (10^{-15} seconds) whereas the emission of a longer wavelength photon and return of the molecule to its ground state takes many magnitudes of time longer, typically occuring in the timespan of several nanoseconds (10^{-9} seconds). The sum of the timespan related to these individual processes defines a parameter known as the fluorescence lifetime τ.[2] The individual steps of the process can visually be represented best through the use of a Jablonski-diagram as seen in figure 1.

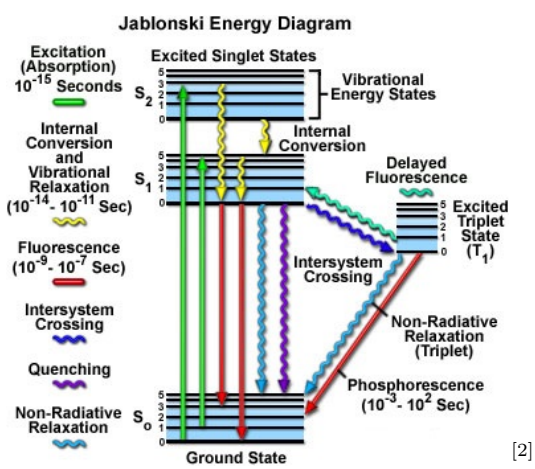

Figure 1: Jablonski energy diagram of the excitation, emission, relaxation and crossing processes of a fluorophore showing their respective directions and durations.

One important extra process present in figure 1 that has not yet been mentioned is that of intersystem crossing. Here, instead of the emission of a photon and the return of the molecule to its ground state, the excited electron crosses over from the excited singlet state into an excited triplet state resulting in the possibility of two different additional processes taking place. First off phosphorescence can occur. The concept of phosphorescence is very similar to fluorescence in that absorbed light is once again emitted at a longer wavelength by the molecule. The essential difference here is that the timescale on which phosphorescence occurs, due to the electron being in the triplet state, can be many magnitudes longer than that of fluorescence (ranging anywhere from several milliseconds to even hours). The other process that can occur, photobleaching, is the irreversible destruction of the fluorescent properties of a molecule due to photochemical destruction or inter-

action with other molecules while the fluorophore is in its triplet state resulting in covalent modification.2 While the average time it takes for a fluorophore to partake in photobleaching varies greatly for different molecular structures and is also strongly dependent on the environment, some fluorophores only emitting a few photons before photobleaching while others can emit millions. Eventually however all fluorophores photobleach.

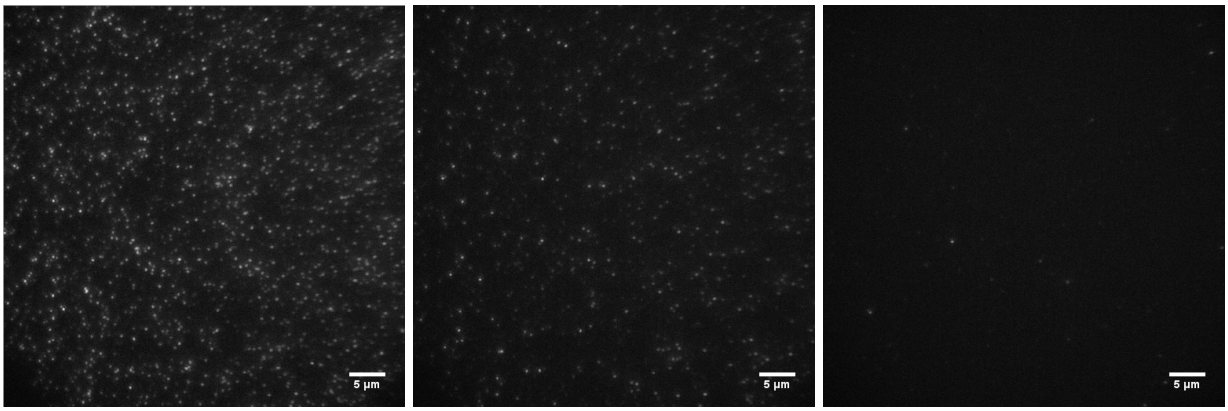

Figure 2: Fluorescence microscopy images of single molecule bleaching in a high concentration (1nM) dried sample of Rhodamine B isothiocyanate. From left to right we see the sample after respectively 1, 10 and 120 seconds of excitation. We can see that after 120 seconds there are barely any fluorescing molecules left as most have undergone photobleaching.

Combined with fluorescence microscopy, fluorophores have a wide range of applications in many fields of science, but are most widely employed in the life sciences such as biochemistry and molecular biology. Here fluorophores are generally applied as non-destructive way of tracking and analysing biological processes on a molecular scale, using the fluorophores as a marker, dye or label through covalent bonding to larger molecular structures such as antibodies.

In this thesis we will investigate a set of photophysical parameters for two types of fluorophores outside of their typical usage environments such as in solution or in biological samples. Rather we will attempt, using PALM techniques, to characterize them under dry conditions. Dry conditions are sub-optimal conditions for most fluorophores, where the quantum yield can drop dramatically and some fluorophores do not even fluoresce. As such these conditions will pose a great challenge in the characterization process. Measurements will be performed on two different types of fluorescent particles: the single molecule fluorophore Rhodamine B isothiocyanate (RITC) and the in-house developed core-shell fluorescent beads (Jantina Particle JP117(2)), which are silica spheres filled with a gold nanoparticle core and a high concentration of RITC.

For our fluorescent particles a set of unique photophysical parameters by which they can be characterized can be defined. These include the average intensity (I) of the particle or ($I(t)$) in the case of fluorescent beads, the photobleaching time τ_{bl} (not to be confused with the fluorescence lifetime τ mentioned before) and for the core-shell particles the populations of the respective intensities. [1]

Starting with the photobleaching time. Under a constant excitation intensity single molecule fluorophores emit a constant intensity, as such photobleaching in single molecules can be detected by the fluorescence simply stopping after a certain period of excitation. Over time the chance of photochemical destruction of the fluorophore due to the excitation intensity increases. On top of that every time the fluorophore is excited from the ground state there is a chance the fluorophore crosses into its triplet state and due to interactions with other molecules also photobleaches. It can then be said that within a certain time span the amount of particles still fluorescing is:

$$dP(t) = -\frac{1}{\tau_{bl}(t)}P(t)dt \tag{2}$$

With P the number of fluorescing particles at time t and τ_{bl} the bleaching time.

If the bleaching time is then to be considered time independent, $\tau_{bl}(t) = \tau_{bl}$, solving the equation results

[1] These parameters were chosen after the ones mentioned in a paper from 2001 by Harms et al.. [3] A universal standard of characterization parameters for fluorophores remains non-existent.

in the standard equation for a mono-exponential decay:

$$P(t) = A \exp\left(-\frac{t}{\tau_{bl}}\right) \tag{3}$$

One can then find that $P(0) = A$ meaning that A would here be the sample's starting number of fluorophores.

Now turning to the fluorescent beads one can expect rather similar results. In principle a fluorescent bead is no more than many single molecule fluorophores put very tightly together and as such we ideally expect it to behave as just an ensemble of normal fluorescent molecules. As the molecules are identical they are expected to emit with the same average intensities and as such the intensity of a simple fluorescent bead can be viewed as the sum of the intensities of many individual particles:

$$I(t) = P(t)I_{sm} = B \exp\left(-\frac{t}{\tau_{bl}}\right) \tag{4}$$

With I_{sm} the intensity of a single molecule fluorophore and $I(t)$ the intensity of the bead at time t.

However due to near-field interactions resulting in metal-enhanced fluorescence (MEF), between the gold nanoparticle core and the RITC particles in the core-shell fluorescent beads used for the measurements, two different discrete intensities and bleaching times are expected, resulting in the intensity following a double exponential decay: [4]

$$I(t) = Ae^{-t/\tau_{bl1}} + Be^{-t/\tau_{bl2}} \tag{5}$$

It is now easy to see that for single molecules τ_{bl} signifies the average time it takes for the amount of particles still emitting light to decrease by a factor of $1/e \approx 36.8\%$, whereas for fluorescent beads it is defined as the average time for the intensity of the particle to decrease to an intensity this same factor of $1/e$ times the original signal.

2 Materials & Methods

2.1 Fluorescence Microscopy

To perform the measurements in this thesis, a wide-field fluorescence microscope setup is used, arguably the most simple form of a fluorescence microscope setup. It is a form of light microscope that instead of using the reflection and absorption of light by a material, uses the fluorescent and phosphorescent properties of a sample to obtain an image of the sample. Light from a light source, in this case an ultra-high pressure mercury vapour lamp, travels through an objective focused on a sample, where it excites the fluorophores or materials that are present. The light is absorbed and subsequently longer wavelength light is emitted by the material, which then travels back through the objective. With the use of a dichroic mirror, a mirror that reflects light of certain wavelengths but is transparent to others, the fluoresced light is separated from that of the original source and is projected onto a detector, camera or into an eyepiece for viewing. [5]

As a fluorescence microscope is a light microscope, it is a diffraction limited system. This means that due to the diffraction of light there is a maximum attainable resolution, proportional to the wavelength of the observed light. The smallest distinguishable feature of an image is then seen as an Airy disk. For a given wavelength of light and numerical aperture (NA) of a lens, one can calculate the airy disk radius:

$$r_{airy} = 1.22\frac{\lambda}{2\text{NA}} \tag{6}$$

When observing particles sized in the range of a hundred nanometers or smaller under an light microscope it is impossible to observe the actual shape or structure of the particles due to this diffraction limit. Using the microscope what will then be detected is a blurred image around the location of the particle called the Point Spread Function (PSF). Depending on the numerical aperture (NA) of the used lens and the wavelength of the emitted light we can approximate the expected diameter of the PSF for the fluorophores.

For the measurements in this thesis a Nikon 60× TIRF oil-immersion objective with a very high NA of 1.49. The higher the numerical aperture of a lens the broader the range of angles under which the system can accept and emit light. This means that for a high NA our PSF is smaller and more strongly peaked allowing for a high resolving power and effective resolution. Oil immersion means that in between the cover glass and the objective a drop of a special clear oil is placed closing the gap between the sample and the top of the objective. The oil used has a refractive index close to that of glass and as such reduces the large difference in refractive index the light usually experiences when travelling from the sample to the lens. Without use of the oil the NA of the lens could never reach such values.

Based on equation 6 an estimation of what radius is to be expected for the fluorophores can be made. For RITC ($\lambda_{em} \approx 570$nm) the airy disk radius is expected to be around 225 to 245 nm. For the core-shell particles we can expect a radius slightly larger by at most 50 nm, depending on the spread of particles throughout the shell.

Of course the detection of a signal from a fluorophore can only occur if the appropriate filters are employed. To gather a usable image one has to filter the excitation light from the lamp from the light emitted by the fluorophore. To give the whole filtering process a bit more context, let us work out the steps that are made when looking at a sample of the fluorophore Rhodamine B in ethanol. Starting with the light source, an ultra-high-pressure mercury lamp is used which has a broad emission spectrum of wavelengths visible to the human eye from around 330nm (ultraviolet) to 800nm (infrared) with various peaks of intensity around 365nm, 405nm, 436nm, 546nm and 576nm (see figure 3). Using various neutral density (ND) filters directly after the light source we can adjust the intensity of the emitted light. For this fluorophore it is known that the absorption peak is around 543nm, the emission peak is around 564nm and that the crossover between the emission and excitation curves takes place around 553nm. The goal is of course to gather as much signal from the fluorophore as possible, meaning ideally one would have a filter set that allows light coming from the source of wavelengths shorter than the crossover to pass, while all light emitted by the sample at wavelengths longer than the crossover is passed through to the detector. As such it is essential to select a suitable set of filters to get as much signal from our fluorophore as possible.

In the microscope setup filter cubes are used (as shown in figure 4) which contain a dichroic mirror and 2 filters; an excitation bandpass and an emission bandpass. Using the mCherry (49008 - ET - mCherry, Texas Red) cube, light from the source first travels through the excitation filter where light of wavelengths between 540nm and 580nm is allowed to pass through (see figure 3). The filtered light is then (largely) reflected off of

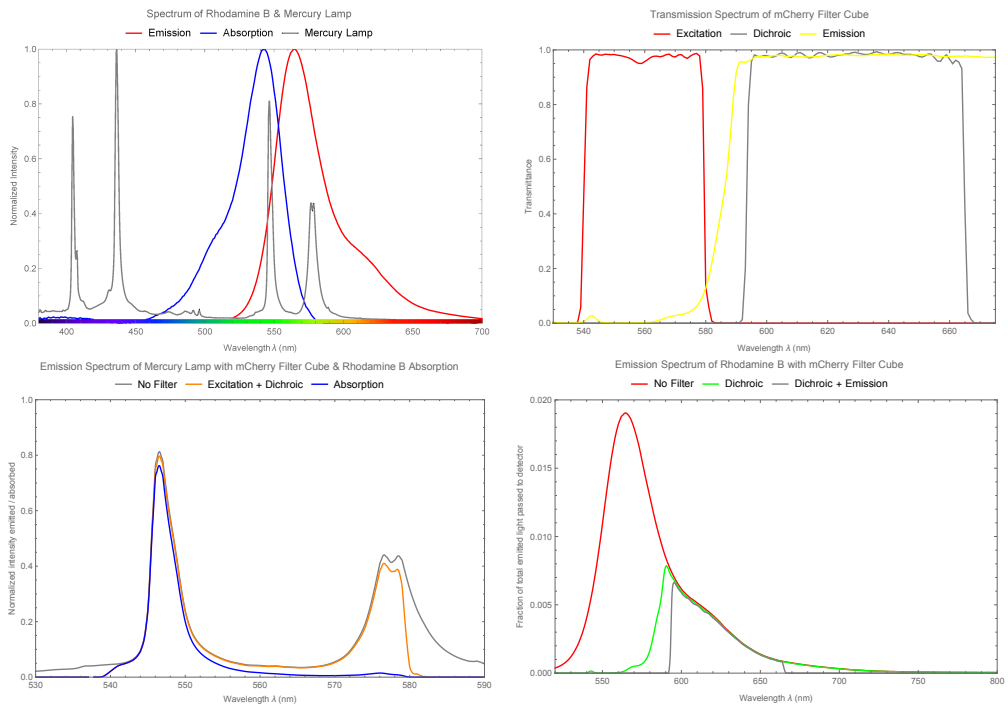

Figure 3: Overview image showing the effects of the mCherry filter cube on the emission spectrum of a mercury lamp and the absorption and emission spectrum of Rhodamine B [6]

the dichroic mirror where the sample is excited. To define the the amount of light that actually gets absorbed by the fluorophore one must look at both the efficiency with which the respective filters and mirrors pass and reflect the light as well as the absorption spectrum of the fluorophore. First the normalized spectrum of the mercury lamp is multiplied by the transmission spectrum of the emission filter. Next, the same is done for the dichroic mirror but using the reflection instead of transmission. Finally this is multiplied by the normalized absorption spectrum of the fluorophore. Using a power meter the intensity of light after having passed both the excitation filter and the dichroic is measured. This means that the integral over the filtered spectrum corresponds to our measured power (results of these measurements are presented in table 2). The integral over the final absorption corrected spectrum should then correspond to the actual intensity of light that is absorbed by the fluorophore. As such the absorption efficiency can then be defined as the fraction of these two values:

$$\eta_{ab} = \int \text{filtered spectrum } d\lambda / \int \text{absorption corrected spectrum} d\lambda \tag{7}$$

To find the emission efficiency the normalized emission spectrum is first divided by its integral to get the percentage of total light emitted at each wavelength. Next the same is done as before, now multiplying by the transmission percentage of the dichroic and emission filter at the respective wavelengths. Integrating this gives us the percentage of the light emitted from the fluorophore that is actually able to reach the detector (η_{em}).

The final step in the efficiency calculation is in the efficiency of the detector. As the detector a very sensitive CMOS-camera is used. Depending on the wavelength of the detected light the quantum efficiency (QE) of the camera changes. The quantum efficiency defines the camera's sensitivity to light and can be interpreted as the percentage of photons hitting the detection that cause it to detect a signal (count). For the CMOS-camera used at the emission wavelengths of Rhodamine B the QE is around 57%. The efficiency of the entire setup, expressed as the detection efficiency (η_d), can now finally be defined as:

$$\eta_d = \eta_{ab} \times \eta_{em} \times \text{QE} \tag{8}$$

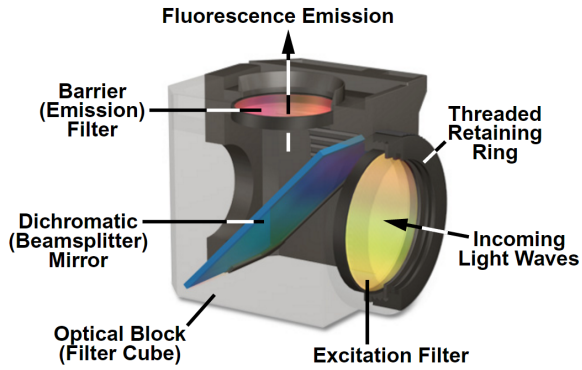

[5]

Figure 4: Cross section of a filter cube showing the combination of different filters and a dichroïc mirror

Assuming the spectrum of RITC to be essentially the same as the spectrum of Rhodamine B but shifted by about +12 nm, we calculate the various efficiencies, the results of which are collected in table 1.

Table 1: Calculated efficiencies for mercury lamp in combination with mCherry filter cube

	mCherry Rhodamine B	RITC
η_{ab}	55.6	65.1
η_{em}	23.2	33.1
η_d	12.9	21.5

Table 2: mCherry filter cube power and intensity measurements

Filter	Measured power	Effective power	Effective Intensity
No filter	2.34mW	1.52mW	$33.1\,\mathrm{W\,cm^{-1}}$
ND 4	0.69mW	0.45mW	$9.8\,\mathrm{W\,cm^{-1}}$
ND 8	0.319mW	0.208mW	$4.54\,\mathrm{W\,cm^{-1}}$
ND 4+8	0.093mW	0.061mW	$1.33\,\mathrm{W\,cm^{-1}}$

2.2 Fluorophore Properties

As mentioned in the introduction, in this thesis measurements will be performed on two different types of fluorophores: Rhodamine-B isothiocyanate ($C_{29}H_{30}ClN_3O_3S$) and JP117(2) (Jantina Particle) core-shell fluorescent beads.

2.2.1 Rhodamine-B isothiocyanate

Rhodamine B isothiocyanate (RITC) is a variation of the widely used fluorophore Rhodamine B with an added isothiocyanate group. Based on the Rhodamine core structure Rhodamine B is a dye that is easily solved in water, ethanol or methanol and is most often used in dye lasers and as a tracer in various aspects of cell biology.

2.2.2 Core-Shell Fluorescent Beads

Stepping away from single molecules we arrive at a slightly more complex type of fluorescent particle: the JP117(2) core-shell fluorescent beads. The JP117(2) is a silica sphere of approximately 100 nm in diameter filled with a high concentration of RITC molecules. In the center the particles contain an approximately 15

nm in diameter gold nanoparticle core. Starting with the synthesis of the gold core, it is first encapsulated in a silica shell (see figure 5). Next the silica shell is grown to around 50nm and the fluorophore is added to the solution and distributes itself around the gold core. Finally the silica shell is grown to its final size after which the fluorophore hopefully spreads out as homogeneous as possible inside the sphere. Compared to single molecules the emission intensities are incredibly high due to the high concentration of fluorophores, also resulting in an expectedly much longer bleaching time. While they may be easier to detect, their characterization process differs slightly and can be trickier as a result of the more complex composition of the particle.

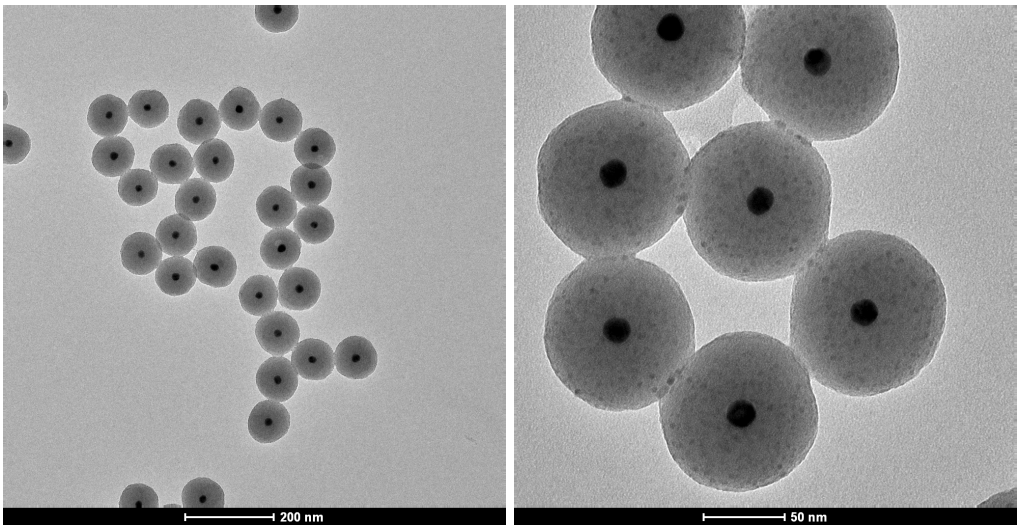

Figure 5: Transmission electron microscopy (TEM) image of JP117(2) core-shell particles. Approximately 100nm in diameter the particles are filled with Rhodamine-B isothiocyanate and a 15nm gold core in the center (seen the image as a black spot). The entirety is encapsulated in a silica shell.

2.3 Sample Preparation

When preparing a sample for viewing under a microscope, it speaks for itself that one is supposed to work relatively clean and organized to ensure a homogeneous sample that is as free as possible from contamination from other sources. It is then not surprising that when preparing a sample of nanoscale fluorescent beads or single molecules the taking of precautions is more essential than ever. The emitted signal from a single molecule fluorophore can (of course depending on the excitation energy and integration time of the signal as well as environmental factors) be incredibly small, ranging in the thousands for the core-shell fluorescent beads and from hundreds to as low as tens of photons per captured frame for the single molecule samples. This means that any contamination can easily hinder the detection of particles by for example decreasing the signal to noise ratio or, even worse, lead to the identification of the wrong particles or signal as our fluorophore.[2] Something which is not hard to imagine happening seeing that, as was discussed earlier, when looking at fluorophores at a molecular level one can not simply make the distinction between different types of particles, as the structure and actual size are impossible to make out.

The preparation starts with the fluorophore itself. Provided as a powder in the case of RITC or in solution in the case of the core-shell fluorescent beads. Several steps are taken of diluting the substance to reach an optimal molar concentration (M) to perform the measurements with. A concentration that is too high can result in self-quenching, the forming of clusters or an overlap in point spread function, preventing proper identification of single sources of fluorescence and leading to high noise levels. Whereas a concentration that is too low will result in measurements where the amount of particles present is not sufficient to perform reliable statistical analysis.

[2]This actually occurred in a retracted 2009 publication in Nature by Wang et al. where signals from single photon emitters due to defects in the glass were misinterpreted as originating from single nanocrystal quantum dots. [7] [8]

Dilution occurs in ultrapure (Milli-Q type 1 standard) filtered water or absolute ethanol to ensure cleanliness of the solution to the highest standard. It was found that for the application discussed in this thesis the ideal concentration is somewhere from 10^{-9} to $10^{-10}\mathrm{mol\,L^{-1}}$. Even here, using solvents purified to the highest standard, one can never be wholly certain that there are no traces of contaminants.

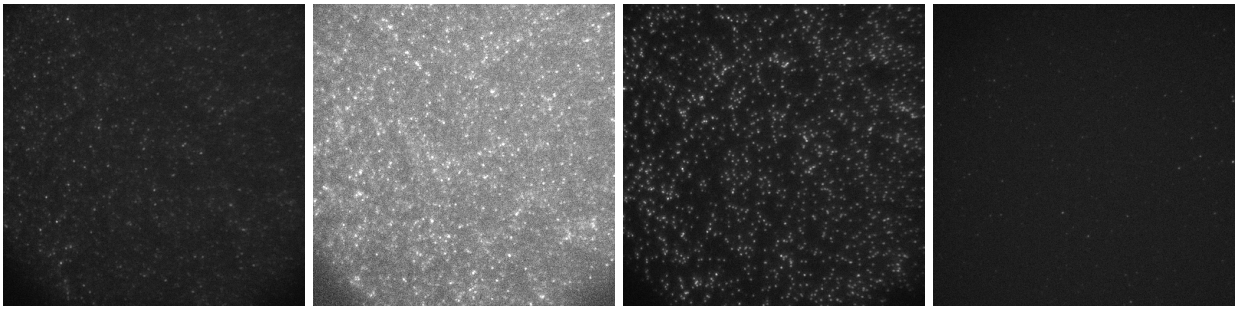

Figure 6: 55.4µm × 55.4µm fluorescence microscopy images showing blank cover glass cleaned in various ways. LR: uncleaned cover glass straight from the packaging; cover glass sprayed with nitrogen gas from the laboratory supply; cover glass spin coated with contaminated milli-Q water; Plasma cleaned cover glass spin coated with clean milli-Q water.

The next step in preparation is the cleaning of the cover glass. Like the solvent the solution is diluted with, the cover glass can be a great source of contamination if not cleaned thoroughly and handled with care. To clean the glass to the standard we desire a plasma cleaner is used. A plasma cleaner is a device where within a (in our case) 20/80 argon-oxygen mixture a plasma is created. If the glass is left in for long enough, this process essentially etches off layers from the cover slip when it is exposed to the plasma. In the end this technique resulted in very clean glass with little contamination and a very low noise level.

Now that the final solutions are ready and our glass is clean the samples can actually be prepared. To prevent clustering the solutions are first left in an ultrasonic bath for around 15 minutes. For single molecules the relatively conventional method of spin coating the particles on cleaned glass is used. The cover slip is attached to the spin coater by a vacuum and over the course of 10 seconds it is sped up to 1500rpm where it remains spinning for 60 more seconds. Applying 100µL of our solution during the 10s ramp resulted in a homogeneous and consistent coating, leaving little to no residue only on the outer most corners of the glass.

Unfortunately our core-shell particles did not adhere to the cover glass at all when using the spin coater. As such the fluorescent beads were applied using a slightly more unconventional method. On the edge of a clean cover slip a 100 µL drop of the solution is placed. Using another clean cover slip the drop is smeared out and left to dry (of course under a cover to prevent interaction with incoming dust or other contaminants in the air) until there is no residue left. Using absolute ethanol as our solvent, little to no residue was left over from this process. On top of that the ethanol also dries a lot quicker.

Finally the cover slip is attached to a glass slide using a special piece of round, double sided tape to ensure a clean seal between the two layers and prevent the introduction of any new contaminants from the air on to the sample. The sample is now finally ready to be viewed under the microscope.

2.4 Data Acquisition and Analysis

Using the CMOS camera connected to a computer, multiple recording series of each type of particle are made for varying excitation intensities. The frame rate is adjusted according to the intensity emitted by a sample as to prevent saturation of the camera. Recordings are saved as a stack of 16-bit 512 × 512 pixel images (one pixel corresponding to an area of 108.3 × 108.3nm), where each pixel contains a value between 0 to 65536, each number representing the number of detected photons (counts) on that pixel.

For data analysis a combination of the existing PALM analysis plugin ThunderStorm for ImageJ and some new custom scripts written in Mathworks Matlab were used.[9] Using ThunderSTORM, particles are localized by approximating their airy disks through an integrated gaussian of the form:

$$\mathrm{PSF_{IG}}\left(x, y \mid \theta_x, \theta_y, \theta_\sigma, \theta_N, \theta_b\right) = \theta_N E_x E_y + \theta_b \tag{9}$$

with:

$$E_x = \frac{1}{2}\left(\frac{x-\theta_x+\frac{1}{2}}{\sqrt{2}\theta_\sigma}\right) - \frac{1}{2}\left(\frac{x-\theta_x-\frac{1}{2}}{\sqrt{2}\theta_\sigma}\right)$$
$$E_y = \frac{1}{2}\left(\frac{y-\theta_y+\frac{1}{2}}{\sqrt{2}\theta_\sigma}\right) - \frac{1}{2}\left(\frac{y-\theta_y-\frac{1}{2}}{\sqrt{2}\theta_\sigma}\right) \tag{10}$$

Where θ_x and θ_y are the sub-pixel molecular coordinates; θ_σ is the imaged size of the molecule; θ_N corresponds to the total number of photons emitted by the molecule; and θ_b corresponds to the background offset.

Having approximated the airy disks with a gaussian function, the σ value of the gaussian fit is expected to be:[10]

$$\sigma = 0.25\frac{\lambda}{\mathrm{NA}} \tag{11}$$

As such the expectation is that for the RITC σ will be around 80 to 100 nm, for the core shell values around 125 to 150 nm are expected.

Now that a dataset has been collected the particles' tracks are traced out. For the tracing of the particles a relatively simple script is used that checks for each consecutive frame whether a particle's location, as given by ThunderSTORM, is within a set distance of a particle's location as found in the previous frame. If such is the case, the particle's index number is added in the data to a list, creating a list-of-lists structure in which each individual list represents a single particle with its data for each frame of the recording. Finally any entries that do not satisfy the requirement of a minimum tracking time are filtered out (effectively reducing the amount of mistracked particles and other sources of fluorescence). Using this method, supposing a neat recording without much clustering and that the particles are well spread out, easily a well defined and comprehensive overview of the movement and locations of the particles on our sample is gathered.

3 Results

Before looking in detail at our characterization results the steps in filtering the data will first be discussed. The basic filtering process for both the single molecules and the fluorescent beads is very similar with the challenge lying mostly in the identification of the individual particles.

First the image series are analyzed with the use of ThunderSTORM. The airy disks of the particles are approximated by an integrated gaussian resulting in 5 relevant parameters for every particle: x-location, y-location, σ of the gaussian, integrated intensity and offset. As ThunderSTORM is a PALM analysis program, particles are localized at sub pixel resolution. Through cross-correlation a correction for any drift that is experienced within the recording is applied. However, as measurements are performed on dried samples without a solvent, drift is rarely in the range of more than tens of nanometers. An early giveaway of sub-optimal particle approximation and samples is a bleaching trend in the offset. As samples are prepared to have as little background signal as possible such a trend would indicate that parts of the particle signal are improperly approximated within our gaussian or that there is a form of contamination.

Next the particle paths in the unfiltered data are traced. Because of the shutter having to be opened by hand, the measurements in the first frame are neglected as they were often found to be to be inaccurate (as such when we refer to the "first frame" in this text it is actually the second frame in the recording). One advantage of the fluorescent beads over the single molecules for analysis is that they still fluoresce strongly even after full exposure to light for several minutes. Any traces that do not last for the full length of the recording series can be immediately filtered out, avoiding identification of signals from sources other than our beads.

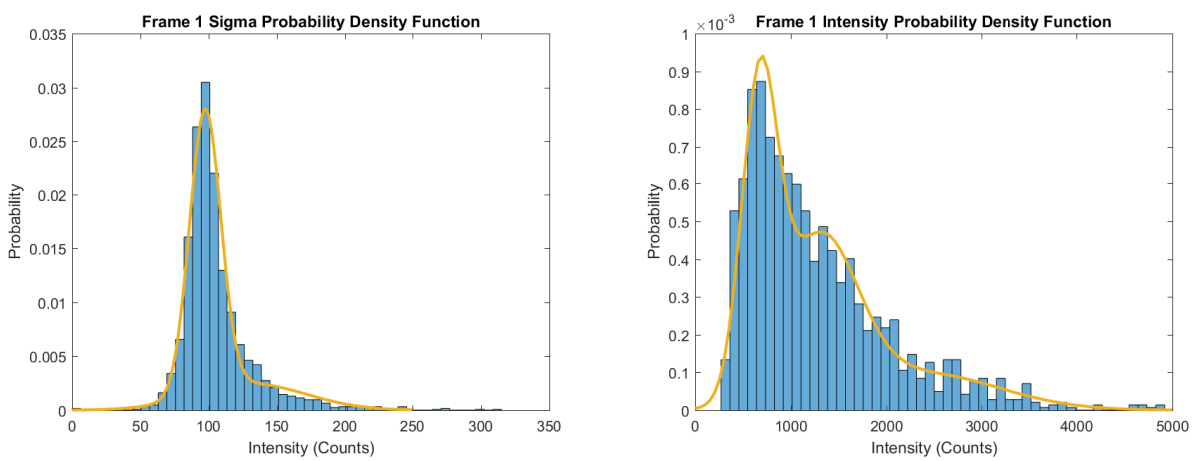

Figure 7: Gaussian mixed probability density functions fit to the distribution of σ and intensity values as found on the first frame of a RITC sample.

In figure 7 the sigma distribution of the traces is plotted as a probability density function. To this distribution a mixed gaussian is fit where the highest peak can be linked to our particles. For RITC samples the value of sigma was found to usually be in the range of 65 to 135 around the Full Width at Tenth Maximum (FWTM) where for the fluorescent beads it was in the range of 130-185. Having now filtered on sigma values the next step is to look at the initial intensity distributions. Large clusters or particles overlapping in PSF have now generally been filtered out but many smaller clusters and contaminations in the range of a few particles still remain, differing only in intensity from single particles and not in σ. As such the same process is applied as with the σ filtering where a mixed gaussian is now fit to the intensity distribution where the gaussian with the lowest mean value is identified as the normal distribution over the single particles (see figure 7. For the RITC samples distributions overlapped quite heavily, making the identification of single particles relatively difficult. Due to the inherent high signal of the fluorescent beads the distribution showed multiple discrete steps in intensity making identification here much easier and precise than was the case with the RITC samples (see figure 8). From here on we shall make a distinction in the analysis and results of both particles.

3.1 Core-Shell Fluorescent Particles

Now that a filtered data set including only single particles has been established, the intensity over time of each individual particle can be mapped. For every frame the mean intensity of all particles is calculated and plotted (represented with red in figure 9). In calculating these intensities we then take the corrected sample standard deviation to be our uncertainty (represented with dashed black lines in figure 9). As discussed earlier in section 1, for a simple fluorescent bead one would expect the intensity to decrease with a factor of $e^{-t/\tau_{bl}}$ over time. It was however found that, as expected, for the structurally more complex core-shell fluorescent beads the mean intensity did not at all decrease as a mono exponential decay but rather to a double exponential decay of the form:

$$I_{jp}(t) = Ae^{-t/\tau_{bl1}} + Be^{-t/\tau_{bl2}} \tag{12}$$

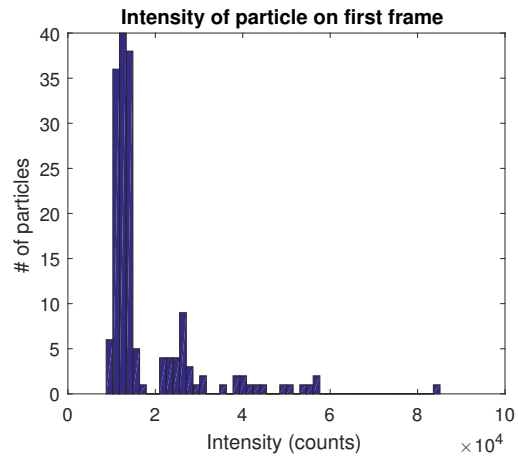

Figure 8: Intensity distribution of core-shell fluorescent particles on the first frame of recording series. Clearly what appear to be discrete steps in intensity can be identified from which it can be gathered the single particle's intensity is somewhere around 1.0×10^4 to 1.8×10^4 counts and that intensities higher than about 2.0×10^4 counts are probably clusters of multiple particles.

From this it can be gathered that the particles show two distinct bleaching times (one shorter than the other): τ_{bl1} and τ_{bl2}. Both the bleaching times are then respectively also related to two different intensities: A and B. For varying excitation intensities of light, measurements were performed and analyzed using the method described, resulting in the multiple plots and fits as shown in figure 9. Fit parameter results from the fits are collected in table 3.

Table 3: Fit parameter values for core-shell particle intensity decay

Filter	No. Particles	Exposure (s)	A (Counts)	τ_{bl1} (s)	B (Counts)	τ_{bl2} (s)
No filter	155	0.05	7604 ± 72	2.51 ± 0.04	19412 ± 75	62.9 ± 0.9
ND 4	51	0.1	9500 ± 105	2.7 ± 0.1	18325 ± 100	112.5 ± 2.4
ND 8	119	0.1	4977 ± 47	3.7 ± 0.1	7636 ± 48	82.3 ± 1.5
ND 8+4	88	0.1	1170 ± 17	7.9 ± 0.2	3473 ± 16	219.9 ± 6.2

Looking at the results in table 3 some conclusions can immediately be drawn. With an increase in the excitation intensity it can be seen that both the values for A and B increase. This is of course an expected effect where an increase in excitation intensity leads to an increase in the amount of absorption and emission cycles that take place resulting in a higher amount of signal per time frame. Furthermore one can see that both τ_{bl1} and τ_{bl2} are inversely related to the excitation intensity (negating the ND4 dataset). This also makes sense as for a higher excitation intensity of a fluorophore the chance of photon-induced chemical damage or covalent modification is expected to also increase. In addition, when a fluorophore undergoes more absorption-emission cycles within a single timeframe the expectation is that it will more often show intersystem crossing into a triplet state within this timeframe and as such show more bleaching due to interactions with other molecules.

Table 4: Characterization parameter results of core-shell particle

Filter	Initial Intensity (Cts./s))	Population A	Population B
No filter	510608 ± 2675	28.1 ± 2.4 %	71.9 ± 0.9 %
ND 4	261830 ± 1873	34.1 ± 1.8 %	65.9 ± 1.3 %
ND 8	119509 ± 889	39.4 ± 1.7 %	60.5 ± 1.4 %
ND 8 + 4	45640 ± 319	25.2 ± 2.2 %	74.8 ± 1.2 %

Adding up both our intensity components A and B we get an approximate initial intensity representing the starting point of our bleaching curve (see table 4). Now comparing the population of both parameters A and B the ratio between appears to remain relatively constant. Averaging values it is found that the population of the faster bleaching component A equals about 32 ± 8 % meaning that the longer bleaching component B shows an average population of 68 ± 8 %.

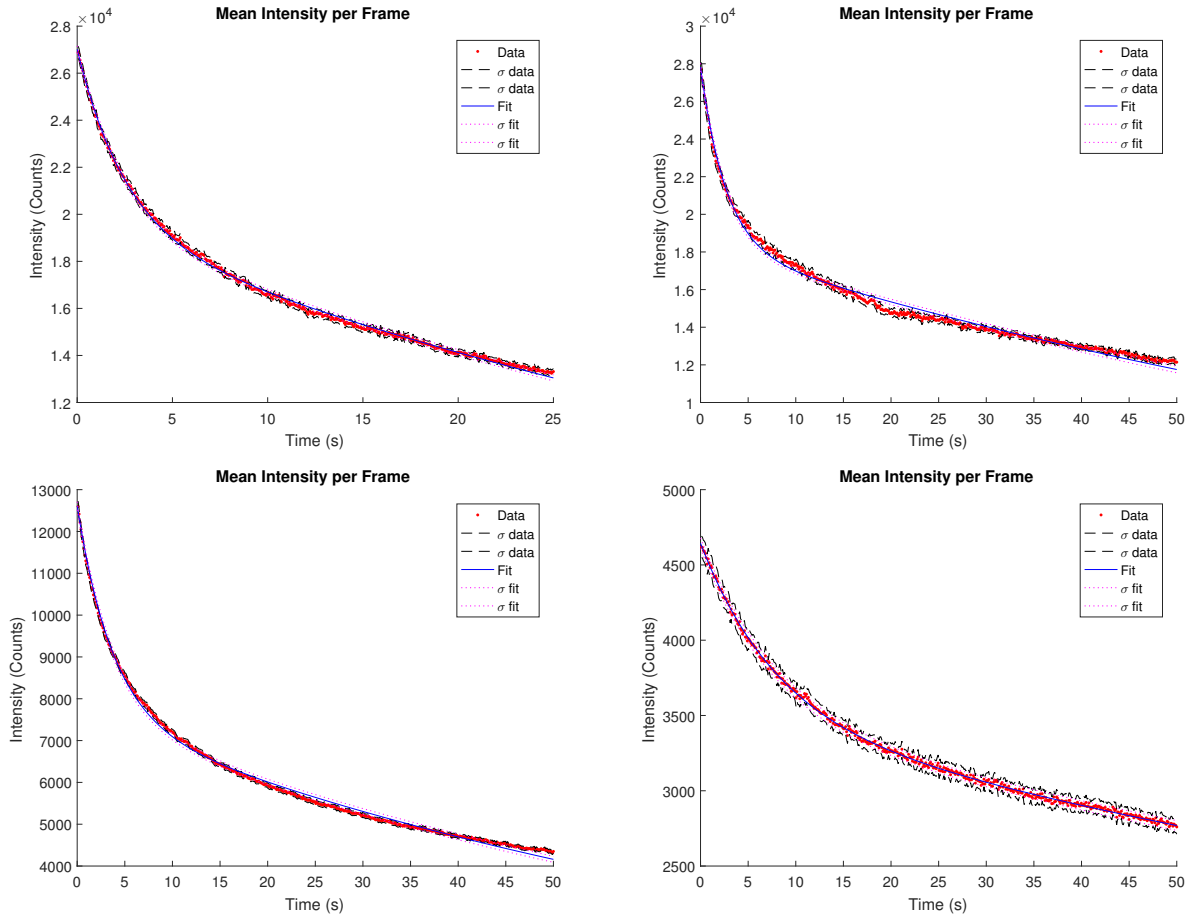

Figure 9: Data and respective fits of the average intensity over time of the core-shell fluorescent particles. Fits were made using a double exponential decay model $I_{jp}(t) = Ae^{-t/\tau_{bl1}} + Be^{-t/\tau_{bl2}}$. LRTB: Datasets of using respectively the filters: No filter, ND4, ND8, ND8+4.

Looking at the fits in figure 9 we can see that for the most part they follow the data points well, residing at most times within the uncertainty bounds of the data. Performing adjusted R-square tests on the fits they are all found to approach a value of one indicating a good fit of the data (the ND 4 fit did seem to show a lower value). Furthermore the root mean squared error values were found to reside close to zero indicating little to no presence of outliers in the data and a fit useful for prediction (the same here goes again for the ND4 fit, deviating a lot more than the other fits). It is however of note that in the fits of the ND 4, ND 8 and filterless dataset we can see that for the last ten seconds or so of the recording the fits consistently predict a value lower than the actual datapoints. Such a deviation can not be observed in the ND 8+4 dataset where the data is arguably best predicted by the fit, residing within the uncertainty bounds of the data at all times.

3.2 Rhodamine B isothiocyanate

Starting again here from the filtered data set one more filter is applied for the RITC samples. In the ideal case the intensity of the single molecules should remain relatively constant until photobleaching, after which the

particle stops emitting light and the trace is stopped. In the intensity curve of clustered particles multiple discrete steps can then be identified (the number of which depending on the amount of particles in the cluster), each step corresponding with one of the particles in the cluster undergoing bleaching. Based on this fact, any traces that show a deviation in intensity higher than around a quarter of the original signal of the trace on the first frame, are removed in an effort to further remove any clusters that earlier slipped through our filtering process.

Next, the intensities of all the particles on each respective frame are added up in an effort to minimize effects from any contaminants that were taken into the data set. From earlier analysis it was found that due to the low signal emitted by the RITC, most contaminants on the sample fall within around the same range of σ and only show a marginally lower intensity than our particles. As such the idea behind adding up the intensities, instead of looking at the amount of particles on each frame, is that the effects on the bleaching curve of the lower intensity particles is then less compared to that of the RITC molecules, minimizing the effect of any unfiltered contaminants on our data.

Having now applied the final filters the data can be fit to a mono exponential decay (as discussed in section 1) of the form:

$$I_{RITC}(t) = Ae^{-t/\tau_{bl}} \tag{13}$$

Inspecting the mono exponential fits in figure 10 one can immediately notice that they deviate rather strongly from the original data points. As such we attempt another fit, this time after the same double exponential model used for core-shell particles:

$$I_{RITC}(t) = Be^{-t/\tau_{bl1}} + Ce^{-t/\tau_{bl2}} \tag{14}$$

Looking at these fits we in figure 10 see that they follow the data trends much better. Applying an adjusted R-square test on the fits they are found to approach a value of one indicating a good fit of the data. Also the root mean squared error values were found to reside close to zero indicating a low presence of outliers and deviation from the fit. Fit parameter results for both fits are collected in table 5. From the results in

Table 5: Fit parameter results for total RITC dataset intensity decay

Filter	Particles	Exp. (s)	A (Counts)	τ_{bl} (s)	B (Counts)	τ_{bl1} (s)	C (Counts)	τ_{bl2} (s)
No filter	952	1	890876 ± 22284	76 ± 3	628805 ± 10540	21 ± 1	506224 ± 11421	127 ± 3
ND 4	1049	1	529906 ± 5299	170 ± 3	216779 ± 22683	51 ± 5	363677 ± 24465	263 ± 18
ND 8	583	2	393541 ± 6624	215 ± 5	205178 ± 9596	59 ± 4	257579 ± 10896	323 ± 12

table 5 we can once again detect the expected inverse relation between the intensity and the bleaching time, where a higher excitation intensity corresponds to a shorter bleaching time. This observation goes for both the mono exponential fits and the double exponential fits. Also once again the idea that a higher intensity excitation corresponds with a higher emitted signal is confirmed in these results.

Table 6: Characterization results for both types of fit

	Mono exponential	Double exponential		
Filter	Intensity (Cts./s)	Intensity (Cts./s)	Population A	Population B
No filter	935 ± 23	1192 ± 37	55.4 ± 1.6 %	44.6 ± 1.1 %
ND4	505 ± 5	553 ± 45	37.3 ± 3.9 %	62.7 ± 4.2 %
ND 8	338 ± 11	397 ± 18	44.3 ± 2.1 %	55.7 ± 2.4 %

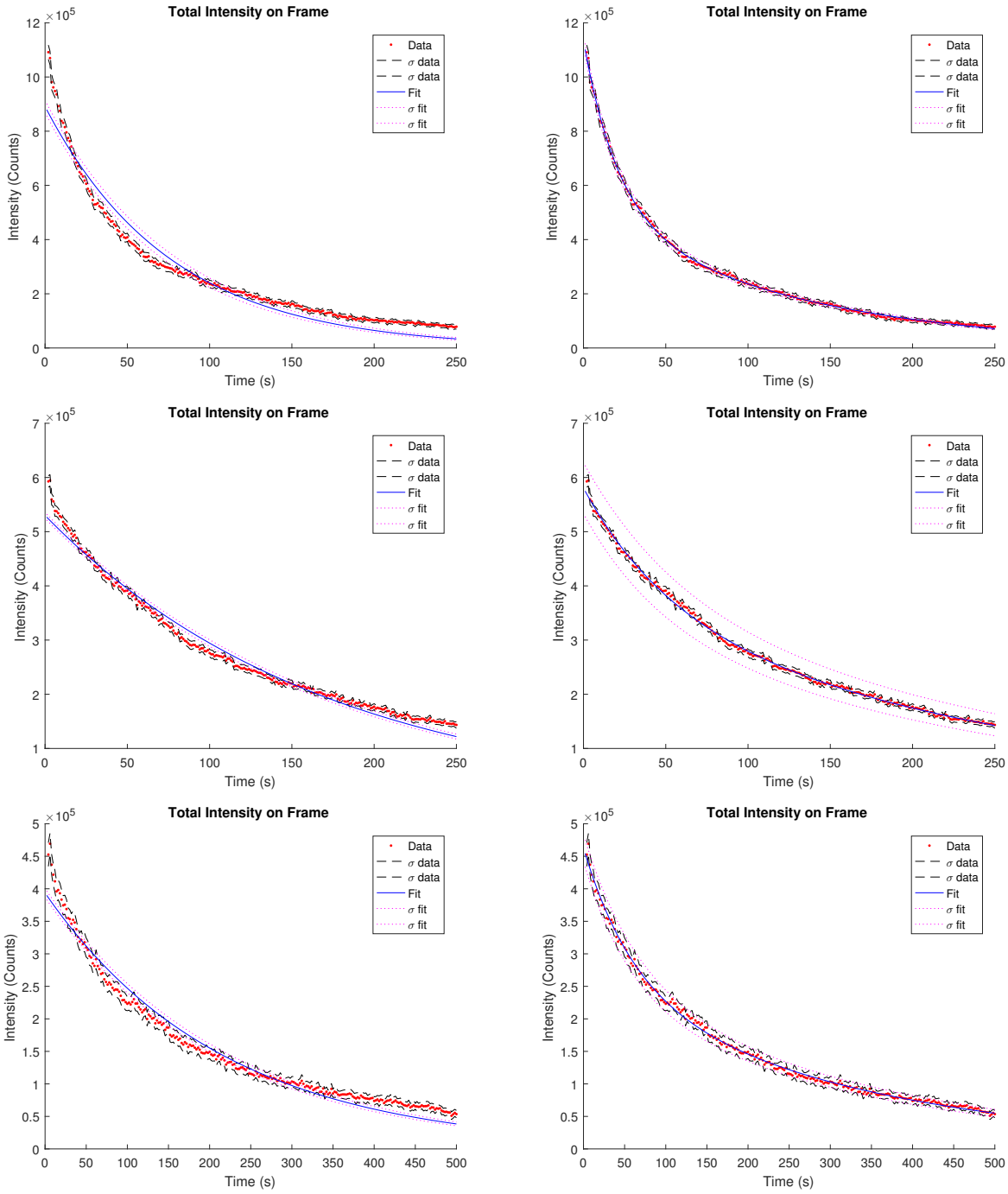

Figure 10: Datapoints and corresonding fits of the total intensity on each frame of the Rhodamine B isothiocyanate samples. Fits on the left were made after a mono exponential decay model $I_{jp}(t) = Ae^{-t/\tau_{bl}}$ while fits on the right follow a double exponential decay model $I_{jp}(t) = Be^{-t/\tau_{bl1}} + Ce^{-t/\tau_{bl2}}$. TB: Excitation by mercury lamp using respectively the filters: No filter, ND 4, ND 8.

4 Discussion

4.1 Core-Shell Particles

For the core-shell particles our expectations were mostly confirmed. Due to the inherently bright nature of the particles they were found to be easily identifiable and provided rather consistent results. Two distinct bleaching times and intensity components were confirmed through the data fitting. The presence of two distinct intensities and bleaching times we ascribe to metal-enhanced fluorescence caused by near-field interaction between the gold nanoparticle core and the RITC particles. As MEF has positive effects on both the intensities and photostability of a fluorophore, the components B and τ_{bl2} are identified as originating from metal-enhanced RITC.

The fits are deemed to be accurate but towards the ends of the recording series it is often noticeable that our fits predict a slightly lower value than the one actually gathered from the data. As MEF is a near-field interaction there is no discrete cutoff for interaction between the fluorophores and metals. Rather the intensity of the MEF related effects is distance dependant. As such to completely model the intensity decay of a particle such as the core-shell particles, one would have to take into account precisely the effects of variations in fluorophore concentrations and the distance-related effects of MEF. For a more general characterization such as in this thesis, the double exponential approach should be sufficient.

4.2 Rhodamine B isothiocyanate

In the end the analysis of RITC proved to be a lot more difficult than initially expected. Due to probably a low quantum yield of the fluorophore under dry conditions signals were found to be very low, resulting in a rather poor signal to noise ratio (as low as 1.5:1 on our lowest excitation intensity) and difficult conditions for separating contaminations on the glass from the particles themselves. Furthermore it was even found that when performing a quick characterization of a few contamination signals, the sigma and intensity distributions often overlapped heavily with that of RITC. On top of this the filtering out of small clusters was found to prove equally difficult with intensity distributions not directly showing any obvious peaks and not conforming much to any normal distributions.

One strange and unexpected phenomenon we noticed with the RITC was that often times particles exhibited blinking behaviour, switching intermittently between an emitting on-state and a dark off-state.While this behaviour is not expected for a fluorophore like Rhodamine it might be attributable to the dried conditions of the fluorophore. Here the probable cause for the very wide intensity distributions can be found. Recordings of the RITC samples were made using rather long exposure times which was necessary due to the very low emitted signal. The blinking behaviour captured over such long exposure times then causes high variance in the intensity captured of a particle on each frame. As such it can be said that ideally a higher intensity light source (probably a laser), and especially a filter set better suited to the spectra of RITC would be preferable to increase the signal, decrease the noise levels and reduce exposure times.

In the end the intensity decay curves did not seem to exhibit much of a mono exponential decay trend, leading any fits of this form to deviate strongly from the acquired data. We expect this to be due to the identification of simply too many particles and clusters as single particles of our fluorophore. The double exponential fits do follow the bleaching trend rather well but for now there is no direct physical explanation for this form of decay. Referring to the opening quote for this thesis one can see that a better fit through adding more parameters does not always yield a more relevant result. This leads us to conclude that the current acquisition setup used is not yet ideal for the single molecule characterization process of Rhodamine B isothiocyanate.

4.3 Single Molecule Contamination

The problem with single molecule analysis really is that you see every single molecule. For every measurement one must keep in mind there is always a chance that the particle that is identified is a contamination.

Leading up to the decision to clean the cover glass by using a plasma cleaner many different attempts at cleaning were made. At first the glass cover slips were washed in 99% ethanol, after which they were sprayed dry using (what was assumed to be clean) nitrogen gas and left in a covered box to dry for another few minutes to completely clean them from residue. Here our first source of contamination was discovered in the

nitrogen gas (see figure 6). As such, avoiding any more use of nitrogen gas, the next attempt involved the use of hydrofluoric acid (HF). HF is a highly corrosive acid capable of dissolving glass. This makes it in principle ideal for cleaning the cover glass as it can basically dissolve the top layer of glass resulting in a, in theory, clean substrate for our sample. Unfortunately it was found that the HF source also had been contaminated, leaving us with samples where we could not be certain whether the signal was from contamination or our fluorophore itself.

Similair problems were encountered with the preparation of the RITC sample dilutions. For example, in one of the earlier samples of RITC what we thought to be signal from our fluorophore was detected, only to later find out that what was seen was actually just signal due to residue left from improperly filtered Milli-Q water (see figure 6). Another attempt, in this case for the core-shell particles, involved using a solution of the polymer polyvinyl alcohol (PVA) as the solvent. Unfortunately this technique turned out to leave much residue, a lot of which even showed fluorescent properties, interfering with the signal from our particles.

In the end it was found that even the eppendorf tubes, used to store and mix solutions in, were a large source of contamination. This actually had such a large effect that purely by amount of contamination it was possible to tell where the tubes were sourced from. To combat this problem, only glass bottles that arrive with a closed lid were used. These bottles did not seem to introduce much if any contaminants.

4.4 Setup and Data Analysis

One of the larger setbacks in this research was the discovery that the lens that measurements had been performed with for weeks turned out to have a crack in it. Originally a 60x plan apochromat oil objective (NA 1.4) was used. Using ThunderSTORM to approximate particle parameters the found intensity and offset levels were rather inconsistent indicating that the gaussian fitting procedure was not performing ideally. As such an extra analysis routine was written which, using the locations of particles as found by ThunderSTORM, approximated the intensity of a particle by directly summing up the counts of the pixels within a radius of the particles. To this data a constrained double exponential decay was then fit of the form:

$$I_{RITC}(t) = A(Be^{-t/\tau_{bl1}} + (1-B)e^{-t/\tau_{bl2}}) + C \tag{15}$$

This then results in the total intensity A; the respective populations B and 1-B; both bleaching times τ_{bl1} and τ_{bl2}; the total offset C. This method seemed to work rather well and gave us at the very least more consistent results than with ThunderSTORM. In the end, after the discovery of the crack in the lens, new data sets were acquired with the replacement lens. These were again analyzed using ThunderSTORM, as for higher concentration samples this technique proved to be a lot more reliable.

5 Conclusion

In this thesis, using four different effective excitation intensities ranging from $33.1\,\mathrm{W\,cm^{-1}}$ to $1.33\,\mathrm{W\,cm^{-1}}$, characterization experiments were performed under dry conditions on both the single-molecule fluorophore Rhodamine B isothiocyanate and the in-house developed, Rhodamine B isothiocyanate filled, core-shell fluorescent particles JP117(2).

For the core-shell particles, the intensity curves were fit to a double exponential, indicating two distinct bleaching time components and corresponding intensity populations, confirming the occurrence of metal-enhanced fluorescence as a result of interactions between the nanoparticle gold core and Rhodamine B isothiocyanate inside the particle. The first component of the double exponential decay is identified as that of the non metal-enhanced particles, showing the shortest bleaching time of 2.51 ± 0.04 to 7.9 ± 0.2 s, depending on the intensity, and a lower intensity population of 32 ± 8 %. The second component, identified as the metal-enhanced particles, shows a longer bleaching time of 62.9 ± 0.9 s to 219.9 ± 6.2 s and a larger intensity population of 68 ± 8 %. With an emission efficiency of approximately 33.1 % and a quantum efficiency of the detector of 57 %, ultimately the intitial intensities of the particles were, depending on the excitation intensity, found to take the values of 510608 ± 2675 to 45640 ± 319 photons/s.

During the Rhodamine B isothiocyanate characterization process, some problems were encountered resulting in rather unreliable results. Due to the extremely low signals from the RITC particles in dry conditions and difficulty in filtering out any contaminants and clusters that showed up on the samples, the particles proved to be very difficult to characterize. This coupled with the fact that long integration times were necessary and particles showed uncharacteristic blinking behaviour resulted in unreliable data. Particles were characterized using three different effective excitation intensities ranging from $33.1\,\mathrm{W\,cm^{-1}}$ to $4.33\,\mathrm{W\,cm^{-1}}$. Using a mono exponential fit to the total intensity decay curves of the samples the bleaching time was found to be between 76 ± 3 and 215 ± 5 s depending on the intensity. The intensity was estimated under the same emission and quantum efficiency as for the core-shell particles to be respectively between 935 ± 23 and 338 ± 11 photons/s.

For further research it would be interesting to see whether the same methods used in this thesis could give more reliable results in single molecule analysis and what the effects of dry conditions would be on fluorophores other than RITC. Using filter sets better suited to the emission and absorption spectrum of RITC or a more sensitive EMCCD camera, signals could in theory be many times higher, increasing the signal to noise ratio and benefiting the characterization process.

References

[1] F. Dyson, Nature **427**, 297 (2004), ISSN 0028-0836, URL http://dx.doi.org/10.1038/427297a.

[2] B. Herman, J. R. Lakowicz, D. B. Murphy, T. J. Fellers, and M. W. Davidson, *Fluorescence excitation and emission fundamentals*, webpage (2017), URL http://www.olympusmicro.com/primer/techniques/confocal/fluoroexciteemit.html.

[3] G. S. Harms, L. Cognet, P. H. Lommerse, G. A. Blab, and T. Schmidt, Biophys J **80**, 2396 (2001), ISSN 0006-3495, 11325739[pmid], URL http://www.ncbi.nlm.nih.gov/pmc/articles/PMC1301428/.

[4] C. D. Geddes, Phys. Chem. Chem. Phys. **15**, 19537 (2013), URL http://dx.doi.org/10.1039/C3CP90129G.

[5] K. R. Spring and M. W. Davidson, *Introduction to fluorescence microscopy*, webpage (2016), URL https://www.microscopyu.com/techniques/fluorescence/introduction-to-fluorescence-microscopy.

[6] H. Du, R.-C. A. Fuh, J. Li, L. A. Corkan, and J. S. Lindsey, Photochemistry and Photobiology **68**, 141 (1998), ISSN 1751-1097, URL http://dx.doi.org/10.1111/j.1751-1097.1998.tb02480.x.

[7] X. Wang, X. Ren, K. Kahen, M. A. Hahn, M. Rajeswaran, S. Maccagnano-Zacher, J. Silcox, G. E. Cragg, A. L. Efros, and T. D. Krauss, Nature **459**, 686 (2009), ISSN 0028-0836, URL http://dx.doi.org/10.1038/nature08072.

[8] X. Wang, X. Ren, K. Kahen, M. A. Hahn, M. Rajeswaran, S. Maccagnano-Zacher, J. Silcox, G. E. Cragg, A. L. Efros, and T. D. Krauss, Nature **527**, 544 (2015), ISSN 0028-0836, retraction, URL http://dx.doi.org/10.1038/nature15745.

[9] M. Ovesn, P. Kek, J. Borkovec, Z. vindrych, and G. M. Hagen, Bioinformatics **30**, 2389 (2014).

[10] S. Stallinga and B. Rieger, Opt. Express **18**, 24461 (2010), URL http://www.opticsexpress.org/abstract.cfm?URI=oe-18-24-24461.